Article

High-Resolution Patterning of Hydrogel Sensing Motifs within Fibrous Substrates for Sensitive and Multiplexed Detection of Biomarkers

Dana Al Sulaiman,[#] Sarah J. Shapiro,[#] Jose Gomez-Marquez, and Patrick S. Doyle*

Cite This: *ACS Sens.* 2021, 6, 203−211

Read Online

ACCESS | Metrics & More | Article Recommendations | SI Supporting Information

ABSTRACT: There has been an increasing and urgent demand to develop nucleic acid bioassays which not only offer high analytical performance but which are also amenable with point-of-care testing. Hydrogels present a versatile class of materials with biocompatible antifouling properties and the ability to be engineered for a range of advanced sensing applications. Fibrous substrates like nitrocellulose offer low-cost and durable platforms to run complex bioassays while enabling portability and ease of handling. We demonstrate herein the ability to synergistically combine these two materials into a portable biosensing platform by leveraging projection lithography. We demonstrate the direct polymerization of hydrogel sensing motifs within a range of fibrous substrates with precise control over their shape, size, location, and functionality. Spatial encoding of the hydrogel motifs enables the multiplex detection of multiple biomarkers on the same test. As a proof-of-concept, we apply the platform to the detection of microRNA, an emerging class of circulating biomarkers with promising potential for early diagnosis and monitoring of cancer. The assay offers a large dynamic range (over three orders of magnitude), high sensitivity (limit of detection of 2.5 amol), as well as versatility and ease of handling. Finally, the bioassay is validated using real biological samples, namely, total RNA extracted from the sera of late-stage breast cancer patients, demonstrating its utility and compatibility with clinical biosensing applications.

KEYWORDS: *fibrous substrate, hydrogel, biosensor, multiplexing, microRNA, liquid biopsy*
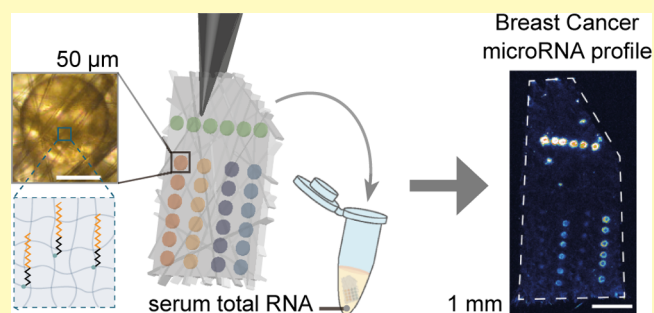
Affordable, sensitive, and multiplex detection of low-abundance biomarkers from biological fluids can transform the way many diseases are diagnosed and monitored. Traditional approaches, however, commonly rely on complex procedures, bulky specialized equipment, and trained personnel in addition to considerable sample or reagent volumes. Hydrogels are a highly versatile class of materials offering biocompatibility, solution-like kinetics, and optical transparency suitable for fluorescence-based readouts.[1−5] They offer attractive matrices for sensing a range of biomolecules including nucleic acids. For example, alginate beads with embedded peptide nucleic acid probes have been used for the sequence-specific detection of nucleic acids through fluorogenic oligonucleotide-templated reactions.[6] Our group has also demonstrated nucleic acid sensing with polyethylene glycol (PEG)-based hydrogels in a range of formats including particles in solution,[3,5,7,8] posts in microfluidic channels,[2,9] and posts in microarrays.[4,10] Hydrogels in these formats, however, are not ideally suited for point-of-care (POC) applications and may be difficult to handle and manipulate, resulting in tedious protocols, sensor loss, and potentially false positive results.

One class of materials that is well suited for the POC is fibrous substrates like paper,[11] silk,[12] and glass fiber.[13,14] Along with

their wicking properties, being durable, affordable, and disposable makes these substrates highly desirable for clinical applications and for use in resource-limited settings.[15,16] Moreover, patterning them in a spatially encoded manner facilitates multiplexing, an important feature for clinical tests.[16,17] In the literature, pre-fabricated hydrogels have been threaded onto yarn substrates and spread on paper to keep reagents hydrated and aid in functionalization.[18,19] Hydrogel precursors have also been printed on paper and nitrocellulose for small molecule detection;[20,21] however, these studies have only demonstrated a resolution over of 100 μm (commonly in millimeters).[22] Achieving high-resolution patterning typically requires expensive technologies or large reagent volumes (≥100 μL) when using more affordable techniques such as bioprinting.[23,24] Although these studies have demonstrated the utility of
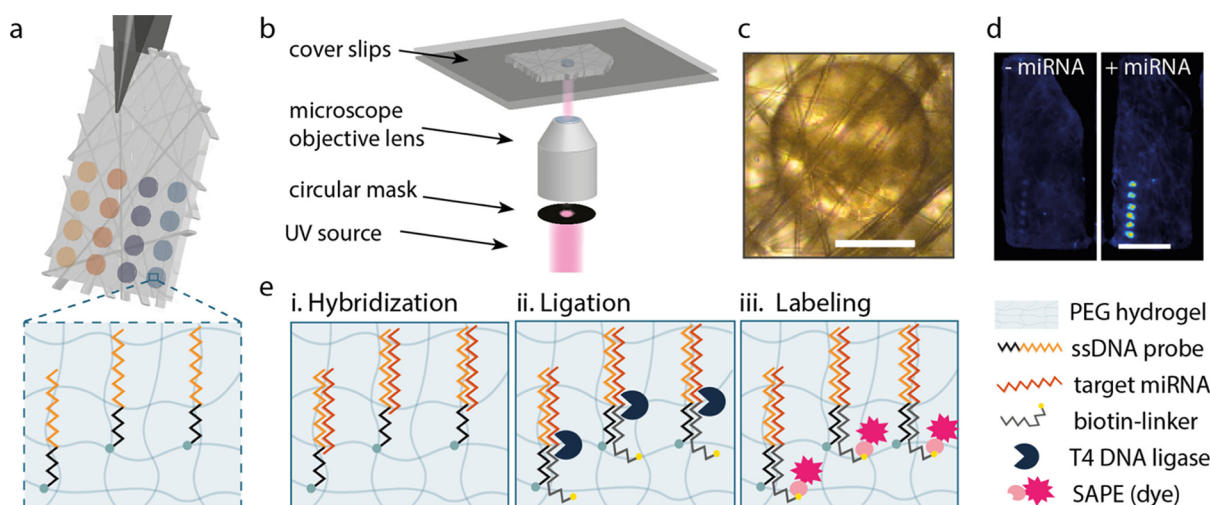
Figure 1. Schematic illustrations of the platform, fabrication process, and sensing strategy. (a) Glass fiber-based platform (2 × 3 mm) with four columns of embedded hydrogel motifs. (b) Platform fabrication with projection lithography. (c) Brightfield microscopy image of a circular hydrogel motif embedded in glass fiber (scale bar 50 μm). (d) Fluorescence scan of two glass fiber substrates after assay completion, in the absence (left) or presence (right) of target microRNA (scale bar 1 mm). (e) MicroRNA sensing strategy within each hydrogel motif.
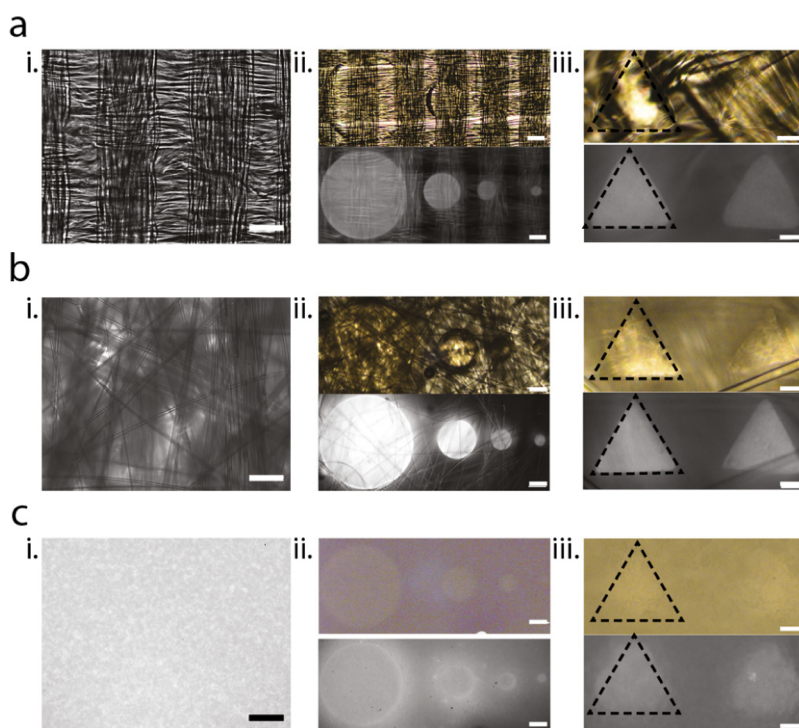
Figure 2. Patterning hydrogel motifs in fibrous substrates: (a) silk, (b) glass fiber, and (c) nitrocellulose. (i) Brightfield images of the substrate microstructure (scale bar 100 μm). (ii) Brightfield (top) and fluorescence (bottom) images of circular hydrogel motifs of radii 250, 100, 50, and 25 μm (scale bar 100 μm). (iii) Brightfield (top) and fluorescence (bottom) images of triangular motifs with dotted line outlining mask shape (scale bar 20 μm).

hydrogels in fibrous substrates, there are no studies, to the best of our knowledge, that show precise high-resolution patterning of hydrogel motifs within fibrous substrates, especially for clinical applications.

Herein, we propose a versatile platform for multiplex detection of biomolecules based on spatially patterning fibrous substrates with microscale hydrogel-sensing motifs (Figure 1). In addition to enabling multiplexing, the fiber substrate acts as a handle to immobilize the motifs and prevent sensor loss (Figure 1a). The format also simplifies buffer exchange for a user-friendly and portable platform. Large dynamic range and high sensitivity are facilitated by a fluorescence readout. To synergistically combine the advantages of fibrous substrates and hydrogels in one platform, we leverage projection lithography.[25] This patterning strategy enables high-resolution features to be created with a range of shapes, sizes, and patterns.

■ RESULTS AND DISCUSSION

A schematic diagram demonstrating the process of patterning hydrogels in fibrous substrates is shown in Figure 1b. Briefly, the substrate was incubated (20 min) in a hydrogel prepolymer

solution, containing the desired bioreceptor molecule. The substrate was then sandwiched between two polydimethylsiloxane (PDMS)-coated coverslips and placed on an inverted microscope stage (20× objective). A photomask of desired shape and size was placed in the field-stop of the microscope. Upon irradiation with UV light through the photomask, a hydrogel motif was generated at the desired location. A brightfield image of a circular hydrogel motif fabricated in a glass fiber substrate is shown in Figure 1c.

Considering the versatility of the fabrication process, it is possible to modify the bioreceptor, the hydrogel, or the properties of the hydrogel to best suit the application of interest. As a proof-of-concept, we have chosen to apply our platform to the multiplex detection of microRNA (miRNA) using a fluorescence-based sensing strategy (Figure 1d). MiRNAs[26,27] are short (~22 nucleotide) non-coding RNA that are of increasing interest for disease diagnosis because of their gene regulatory functions, dysregulated patterns in many diseases[28,29] including cancer[30–34] and stability in biological fluids.[35,36] Herein, miRNA detection is enabled by covalently incorporating an acrydite-modified ssDNA capture probe into the hydrogel during polymerization (Table S1 for probe sequences). The assay, based on previous work by our group, consists of three steps: (i) hybridization of the target miRNA to the ssDNA, (ii) ligation of a biotinylated linker, and (iii) labeling with streptavidin conjugated to a fluorophore (streptavidin–phycoerythrin, SAPE) for fluorescence visualization (Figure 1e).[7] To demonstrate the ease of extending this platform to other classes of biomolecules, we also applied it to protein detection by capturing thyroid-stimulating hormone on antibody-functionalized hydrogels embedded in glass fiber substrates (Figure S1).

Screening Fibrous Substrates. Incorporating hydrogels into fibrous substrates can leverage the durability and wicking properties of the substrates while maintaining the functionality and biocompatibility offered by the hydrogels.[1] To find a suitable substrate for our assay, we screened through three low-cost and commercially available substrates:[12,14,37] nitrocellulose, glass fiber, and silk. Nitrocellulose is commonly used as a substrate for both lateral flow and dipstick assays,[37] while glass fiber is often used in the sample pad or conjugate pad of lateral flow assays[14,15,38] or can be functionalized for microfluidic assays. Silk has also been used as a microfluidic platform for biomolecule detection.[39] Each fibrous material presented a different microstructure (Figure 2(i)). Silk had a highly ordered structure (Figure 2a), while the glass fiber was more amorphous (Figure 2b). Nitrocellulose also displayed random pores but of a smaller pore size (Figure 2c). Within each substrate, we fabricated circular hydrogel motifs using masks with projected radii of 250, 100, 50, and 25 μm (Figure 2(ii)). Fluorescent microspheres (Polyscience Inc.) were physically entrapped within the hydrogel pore structure for visualization. As seen in the brightfield (above) and fluorescence (below) images, motifs were visible in all substrates (Figure 2(ii)); however, the circles were more well defined in silk and glass fiber compared to nitrocellulose.

We next patterned triangular shaped motifs in the three substrates to investigate patterning resolution and sharpness of the motif edges (Figure 2(iii)). Although the motifs were identifiable in all substrates, motifs in the glass fiber had the most well-defined shape compared to the photomask (Figure 2b). Quantitative analysis of the results can be found in Figure S2, where signal-to-noise ratio was calculated for each substrate.

The substrate-specific variation can be attributed to light scattering induced by the substrate during the polymerization process, which reduces the amount of UV light penetrating the substrate and, thus, the extent of polymerization. To verify this, we measured the percentage light transmittance of 365 nm light for all substrates using a Thorlabs PM100USB light intensity meter (Figure S3). Glass fiber and silk transmitted similar amounts of light at 49% and 51%, respectively, while nitrocellulose only transmitted 22%. It is noteworthy that the thickness of the silk was less than half that of the glass fiber, so the transmittance per unit depth was much higher for the glass fiber, which may account for the better shape definition.

Characterization and POC Properties. Glass fiber membranes are chemically inert materials composed of fine fibers of glass organized in a mesh-like structure. Glass has traditionally been exploited in microfluidic chips because of its desirable mechanical, electrical, and electro-osmotic properties,[13,40] in addition to high wettability and hydrophilicity when compared to nitrocellulose.[12] Because of the fibers' brittle nature, this substrate can also be cut with a regular cutting blade and precisely patterned with a laser cutter. Because of these properties and optimal patterning resolution, glass fiber was used in all further studies and investigated as a potential substrate for POC bioassays.

First, we examined the ability to fabricate hydrogel motifs of varying structures, such as strips analogous to the test lines used in lateral flow and dipstick assays.[37] With a 20× objective lens, we successfully fabricated hydrogel lines that stretch ~1 mm across the substrate (Figure 3a, left) using only 5 μL of the
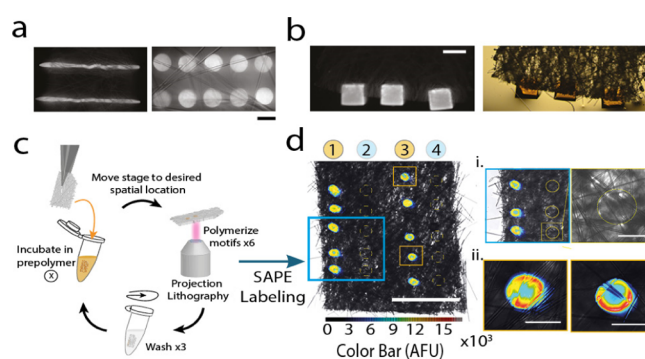
Figure 3. (a) Hydrogel motifs as strips (left) and arrays (right) in the glass fiber substrate (scale bar 50 μm) and (b) fluorescence (left) and brightfield (right) images of square motifs hanging off the substrate edge (scale bar 300 μm). (c) Multiplexing protocol. (d) Overlay of fluorescence (color) and brightfield (greyscale) scans of a 4-plex substrate (scale bar 1 mm). Magnification of a blank motif (i) and two fluorescent motifs (ii) (scale bar 100 μm).

hydrogel prepolymer solution. By using lower magnification or contact lithography,[41] we anticipate patterning even larger structures in the substrate. We were also able to pattern smaller motifs in fine arrays with good uniformity and an interparticle coefficient of variation in a fluorescence of 17.6% (Figure 3a, right). This configuration is useful in bioassays to generate statistics from a single sample.

Next, for dipstick-like assays, it is important that the substrate can also be utilized as a handle for sensing motifs. To investigate this, we polymerized 300 μm biotin-functionalized squares at the edge of a glass fiber substrate, then labeled them with SAPE for imaging (Figure 3b). Interestingly, the fluorescent signal of the square motif area on the substrate was comparable to that which
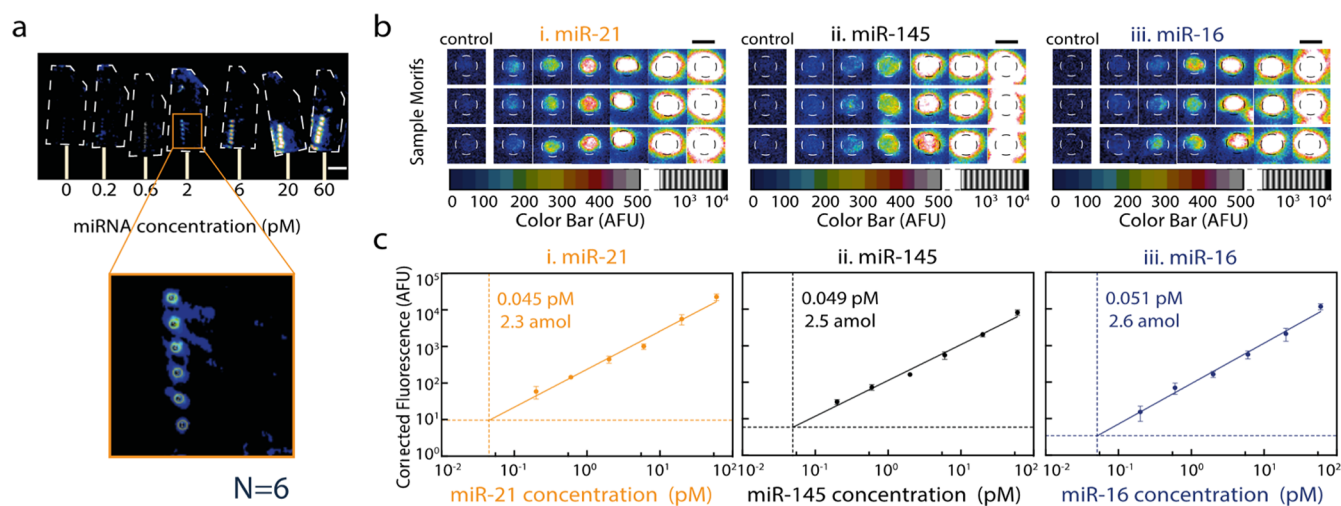
Figure 4. Investigating platform sensitivity with breast cancer-specific miRNAs. (a) Seven fibrous substrates used in the calibration curve, with a magnified view of circular regions of interest (50 μm radius) around each motif used in image analysis (Fiji ImageJ). (b) Fluorescence scans of three select motifs at each concentration, with high contrast color bar below (for visualization purposes). (c) Calibration curve of the corrected fluorescence vs miRNA concentration on a log−log scale, with curve fitting, and limit of detection (LOD) for miR-21, miR-145, and miR-16.

was overhanging the edge (Figure S4). This indicated that both the polymerization and signal acquisition were similar within and outside the glass fiber substrate. The hydrogel motifs also remained immobilized on the substrate even in this configuration, validating the platform's durability for portable bioassays.

Finally, to investigate multiplexing capability, we designed a 4-plex assay format where each column of motifs would be made from a different prepolymer solution; herein, biotin-labeled, blank, biotin-labeled, then blank for columns 1, 2, 3, and 4, respectively. Considering the top-right cut corner as an orientation marker, the column's position (from the left) would spatially encode the target biomarker in the final assay. Fabrication involved repeating the following series of three steps for each column: (i) incubation of the substrate in the desired prepolymer solution (20 min), (ii) polymerization of motifs in a single column at a specified spatial position, and (iii) rinsing off unreacted prepolymer solution (Figure 3c). After labeling and imaging, the fluorescence was only observed in columns 1 and 3 indicating the absence of cross-contamination between prepolymer solutions, efficient washing between cycles, and the ability to multiplex. For visualization purposes, we overlaid the fluorescence and brightfield images of the assay to show the edges of the fibrous substrate (Figure 3d). A yellow circle (50 μm radius) was used to outline the hydrogel motifs (containing blank prepolymer solution) in columns 2 and 4 (Figure 3d(i)). With high magnification and a high contrast color map (for visualization purposes), it was possible to visualize layers of the glass fiber surrounding and immobilizing each hydrogel motif [Figure 3d(ii)], whose structure and thickness were further characterized by confocal microscopy (Figure S5). Consistent results (i.e., no cross-contamination) were observed when the latter experiment was repeated with prepolymer solutions containing two different fluorescent dyes (Figure S6).

Application to miRNA Detection. Before applying the platform to biomolecular sensing, we optimized other assay parameters including motif size and exposure time to ensure maximum signal-to-noise ratio (Figure S7). A 50 μm radius hydrogel motif and 300 ms exposure time generated the greatest signals, so these parameters were used for miRNA assays.

miRNAs have become increasingly important diagnostic targets because of their dysregulated expression profiles in cancer[42−44] and their stability in body fluids.[35,36] For this proof-of-concept study, we chose the following panel of miRNAs: miR-21, miR-145, and miR-16 as their serum expression levels have been shown in the literature to be significantly dysregulated in breast cancer patients compared to healthy controls.[45,46] In particular, miR-21 is one of the most significantly upregulated miRNAs in breast cancer.[47] It acts as an oncogene and is associated with advanced cancer stage[48] and poor prognosis.[49,50] Conversely, miR-145 acts as a tumor suppressor and is downregulated in breast cancer patients.[47] Lastly, miR-16 serum expression levels are significantly higher in breast cancer patients compared to healthy controls.[51] It is noteworthy that there is controversy in the field regarding miR-16 as many other studies have identified it as an endogenous control because of its stable expression across healthy and diseased individuals.[52−56]

To investigate the sensitivity of miRNA detection, we prepared calibration curves of fluorescence versus target concentration from 0.2 to 60 pM, equivalent to 10−3000 amol (Figure 4a). This range covers the concentrations expected for endogenous circulating miRNA (high femtomolar to picomolar regime).[57−59] The concentration of ssDNA probes in the prepolymer solutions was chosen based on previous studies to ensure rate-matching of the binding of miRNA targets.[60] These concentrations were 247, 50, and 100 μM for (i) miR-21, (ii) miR-145, and (iii) miR-16, respectively. Figure 4b displays the fluorescence intensity of three randomly selected motifs for each concentration with a black circle outlining a 50 μm radius around each motif. Because of the large dynamic range of fluorescence—spanning 4 orders of magnitude—it was not possible for each concentration to be individually represented by one color in the false colored images (see color bar, Figure 4b).[52−55]

Calibration curves, as shown in Figure 4c, display the mean corrected fluorescence intensity for each miRNA concentration. The intensities were corrected by subtracting the mean intensity of the control condition (0 miRNA). The curves, plotted on a log−log scale, appeared linear over more than three orders of magnitude. Data analysis of these results involved fitting a power
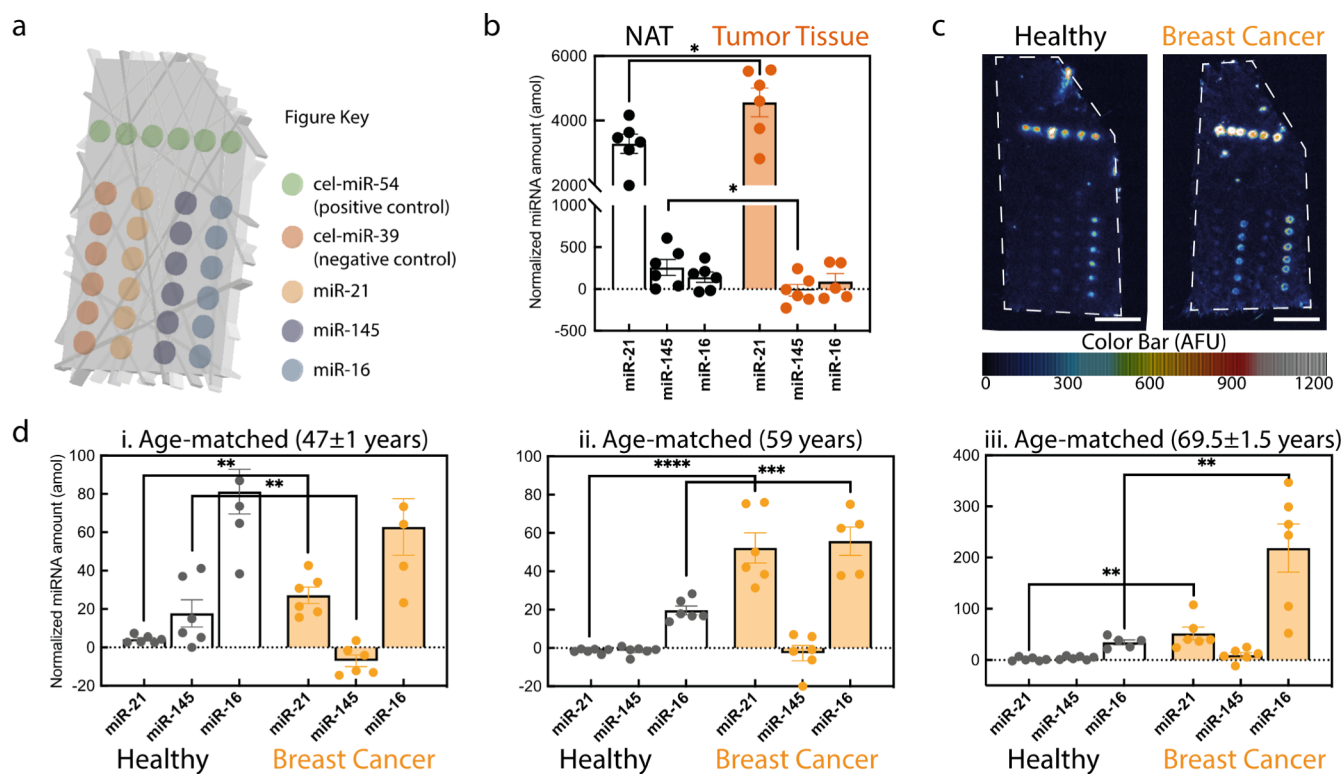
Figure 5. Platform validation with total RNA from biological specimens. (a) Diagram of spatially encoded 5-plex platform design targeting 2 control and 3 endogenous miRNA. (b) Normalized miRNA amount in NAT vs tumor tissue from breast cancer patient. (c) Fluorescence scan of substrates from healthy and breast cancer patient serum, with characteristic up−down−up trend in columns 2−3−4 for cancer patient. (d) Normalized miRNA amount in the serum of age-matched healthy and breast cancer patients (* indicates significance from *t*-test). Each graph contains data from one patient and healthy control with error bars representing standard deviations from multiple hydrogel motifs on a single substrate.

law in the form of $y = Ax^b$ to the data, with R^2 of 0.986, 0.989, and 0.991 for miR-21, miR-145, and miR-16, respectively (Table S2). The LOD, calculated[61] as three times the standard deviation of the control condition, was 2.3, 2.5, and 2.6 amol for miR-21, miR-145, and miR-16, respectively (Table S3). This is equivalent to an LOD of ∼50 fM which represents a sensitivity sufficient for the detection of miRNA from biological samples.

Previous research from our group has shown that maximal signal intensity (I_{max}) can be reached by minimizing the total sensing area, which herein is a product of hydrogel motif area (A_m) and number of motifs (N_m).[62] Because our optimal motif radius was 50 μm ($A_m = 785$ μm^2), I_{max} could be maximized by reducing N_m. We have chosen an N_m of 6 to maximize the signal while enabling statistical analysis. Considering I_{max} is inversely proportional to N_m and particle assays typically have $N \sim 50$ (to account for particle loss), reducing N_m could theoretically improve I_{max} by one order of magnitude. Commercially established detection methods such as the reverse transcription polymerase chain reaction or microarrays have detection limits around 10 aM to 20 aM[63,64] and 10 fM to 40 pM,[64,65] respectively, but require complex equipment and a complicated primer design. Furthermore, microarrays typically require long incubation times ∼12 h for hybridization while our assay takes ∼4 h. Compared to other miRNA POC technologies such as colorimetric lateral flow assays (LOD ∼ 60 pM), this platform provided up to 3 orders of magnitude improvement in sensitivity.[66,67] Compared to other optical sensors (based on surface plasmon resonance[68] or fluorescence-based AuNP[69] and quantum dots[70]), this platform offered a better or equivalent LOD, typically ranging from 10 fM to 10 pM (Table S4).[69−73]

Furthermore, because of the hydrogel's nonfouling properties, this platform is also amenable to miRNA detection directly from biological samples,[3,74] and this will be explored in future works.

Validation with Breast Cancer Specimens. To demonstrate its utility in clinical testing, we sought to validate the platform with endogenous RNA from biological specimens. For these studies, a 5-plex substrate layout was designed, consisting of one horizontal row and four vertical columns, each with 6 hydrogel motifs (Figure 5a). The horizontal row targeted cel-miR-54, the positive control which was spiked into the samples at 1000 amol. The first vertical column targeted the negative control, cel-miR-39. The second, third, and fourth columns targeted the breast cancer biomarkers miR-21, miR-145, and miR-16, respectively. This order was chosen such that breast cancer patients would exhibit a characteristic up−down−up trend of fluorescence in columns 2−3−4. The columns encode the miRNA profile, and the trend could be used to qualitatively identify cancer patients from healthy controls, even before quantitative analysis.

First, the platform was used to detect miRNA expression from 500 ng of total RNA extracted from the breast tumor tissue and normal adjacent tissue (NAT) of a single patient (BioChain). Fluorescence values were corrected by subtracting the mean fluorescence of the negative control then normalized by the positive control to obtain the attomole amounts of miRNA (details in Method S1). The results shown in Figure 5b were consistent with the literature, wherein miR-21 was upregulated[47,48,75−77] and miR-145 was downregulated[47,75,76,78] in the breast tumor compared to NAT (*p*-values of 0.038 and 0.043, respectively) (Table S5).[54] For POC diagnostic applications, we

could use these expression levels to set thresholds for expression levels of miR-21 and miR-145 to identify diseased and healthy individuals. To get more reliable limits, we would need a clinical study with a larger sample size, which is beyond the scope of this paper. Interestingly, no significant difference was observed in miR-16 between the two tissue types. This result is in-line with the studies considering miR-16 as a stable endogenous control miRNA.[52−56]

Next, we investigated the ability to detect lower amounts of circulating miRNA extracted from the sera of breast cancer patients. In particular, we have chosen female Caucasian breast cancer patients ranging from 46 to 71 years of age, at similar stages of disease (UICC stage T2N2 or T2N3), and whose serum samples were collected prior to surgical removal of the primary tumor (Table S6 for donor details).

The control group consisted of age-matched female Caucasian healthy patients. Total RNA was purified from 200 μL of x donor serum using the Qiagen miRNeasy Serum/Plasma Advanced Kit. The purified RNA was eluted into 37 μL of 1× TE. While 2 μL of this was used for characterization and quality control using a NanoDrop Spectrophotometer (Table S7), 32.5 μL was used in the miRNA assay.

Figure 5c shows the fluorescence scan of the fiber substrates from age-matched (69 ± 1.5 years) healthy (left) and breast cancer patient (right). Even before data normalization and analysis, the characteristic trend of up−down−up in columns 2−3−4 was observed in the breast cancer patients, while it was not observed in the healthy controls. Another notable observation was the difference in the fluorescence of the positive control cel-miR-54 between patients, emphasizing the importance of data normalization to account for RNA extraction efficiency. The attomole levels of each miRNA were quantified and plotted in Figure 5d for the three sets of age-matched patients: (i) 47 ± 1, (ii) 59, and (iii) 69 ± 1.5 years. Again qualitatively, the characteristic up−down−up trend was observed in all breast cancer patient miRNA profiles (orange). Quantitatively, miR-21 was upregulated in all breast cancer patients compared to their respective controls (p-values of 0.00035, 0.000044, and 0.0022 for (i), (ii), and (iii), respectively), as is consistent with the literature. Also consistent with the literature, in patient set (i), miR-145 was downregulated in the breast cancer patient (p-value = 0.0093). However, no significant difference was observed in the other patient sets. This was attributed to the low levels of endogenous miR-145 in the serum, which were too close to the LOD of the platform. Based on our prior work with gel particles bearing a similar probe design, rolling circle amplification could be seamlessly incorporated in the future and is expected to improve the LOD by at least one order of magnitude, enabling a more reliable detection of such low expression miRNA.[79] In patient sets (ii) and (iii), miR-16 was upregulated in breast cancer patients (p-values of 0.00071 and 0.0065, respectively); however, no significant difference was observed in patient set (i). This result echoes the controversy in the literature regarding miR-16 as an upregulated biomarker or stable control miRNA.

CONCLUSIONS

We report herein the first demonstration, to the best of our knowledge, of amplification-free multiplexed detection of 3 endogenous circulating miRNA and 2 control miRNA on a fibrous substrate. The platform is highly versatile, facile, and amenable with POC testing. Further probes can be readily introduced on the platform to detect other miRNA or even protein biomarkers. Importantly, the work presents reliable quantitative values for miRNA in the human serum, which is difficult with amplification-based techniques (e.g., relying on cycle threshold or C_t values from PCR).[54,56] The platform offers high sensitivity (2.5 amol LOD) and utility even with real biological samples. With a reliable platform and well-controlled conditions, it was possible to consistently detect endogenous miRNA and observe a characteristic miRNA profile in all breast cancer patients. By increasing multiplexing, it will be possible to visually encode more complex miRNA profiles and potentially detect different cancer types through liquid biopsy tests, as an alternative strategy to invasive tissue biopsies for cancer diagnosis and monitoring.

EXPERIMENTAL SECTION

Fibrous Substrates. The substrates in this study were glass fiber (G041 Glass Fiber Conjugate Pad Sheet, Millipore), nitrocellulose (FF120HP, Whatman), and silk (Figure S8). Substrate thickness, measured using a digital micrometer (Tormach), was 202 μm for the glass fiber, 195 μm for the nitrocellulose, and 85 μm for the silk.

Hydrogel Prepolymer Preparation. Hydrogels were based on poly(ethylene glycol) diacrylate (PEGDA). For characterization studies with fluorescent microspheres, the monomer solution consisted of 35% PEGDA 700 (Sigma), 20% PEG 200 (Sigma), 5% photoinitiator (2-hydroxy-2-methylpropiophenone, Sigma), 35% 3× Tris−EDTA buffer (Calbiochem), and 5% fluorescent microspheres (carboxylated YG, 0.2 μm diameter, Polyscience, Inc.). For bioassays, the monomer consisted of 20% PEGDA 700, 40% PEG 600, 35% 3× Tris−EDTA buffer, and 5% photoinitiator. PEG 200 was used for protein detection. The monomer solution was then diluted 9:1 with the probe. For studies with the biotinylated probe, the final probe concentration in monomer was 10 μM, while for miRNA studies, it was 100 μM unless otherwise indicated. All probes were ordered from Integrated DNA Technologies (sequences in Table S1).

Patterning Hydrogels in Fibrous Substrates. To create hydrogel motifs, the substrate was incubated in 50 μL of the desired prepolymer mixture (20 min) then sandwiched between two PDMS-coated cover slips. The cover slips were placed on an inverted microscope (Zeiss Axio Observer), and hydrogel motifs were individually polymerized using projection lithography. To do this, a mask (Fineline Imaging) of the desired shape and size was placed in the field stop of the microscope, then UV light (UV LED, Thorlabs M365L2-C4) was projected through the photomask and a Chroma Technology 11000v3-UV filter set. The substrate was then rinsed thrice in 1× Tris−EDTA buffer with 0.05% Tween-20 (1× TET). For multiplexed assays, the process of prepolymer incubation, polymerization, and rinsing in 1× TET was repeated with a different prepolymer mixture, each time changing the location of motifs to spatially encode the probe. Unless otherwise specified, an exposure time of 300 ms was used, using a Vincent Associates Uniblitz VCM-D1 shutter driver controlled by a Python script. After all motifs were polymerized, an oxidation step was next performed to increase the hydrophobicity of the hydrogel motifs and reduce nonspecific binding. This was performed by incubating substrates in 500 μM potassium permanganate (Sigma) in 0.1 M Tris-HCl buffer (pH 8.8) for 5 min. After rinsing thrice in 1× TET, substrates were left overnight in 1× TET at 4 °C before running the assay.

Biotin−Streptavidin Assay. For the biotin−streptavidin assay, 50 μL of 1× TET buffer with 50 mM NaCl (rinse buffer, or RB) were placed in a tube, to which 5 μL of SAPE (20 μg/mL in RB, Life Technologies) was added. The patterned substrate was then added to the tube and the tube was placed on a thermoshaker (MultiTherm Shaker, Thomas Scientific) for 45 min at 21.5 °C and 1500 rpm. After incubation, the substrates were washed thrice by replacing all liquid in the tube with 500 μL of RB.

miRNA Detection Assay. For synthetic miRNA assays, a hybridization tube was prepared with 40 μL of hybridization buffer (427.5 mM NaCl in 1× TE) and 5 μL of the synthetic target in 1× TE.

For endogenous total RNA, the hybridization tube contained 32.5 μL of the eluant in 1× TE and 17.5 μL of hybridization buffer (1 M NaCl in 1× TE). For endogenous RNA, the hybridization tube was heated on a thermoshaker (90 °C, 1500 rpm, 5 min) then allowed to cool down gradually to 55 °C. For hybridization, the substrate was placed into the tube and heated on a thermoshaker (55 °C, 1500 rpm, 90 min). For ligation, the substrate was rinsed thrice in RB then placed in a ligation buffer containing 0.05% Tween-20, 8.8 mM NaCl, 33 nM A12 universal linker (Integrated DNA Technologies, Table S1), 8% (v/v) NEBuffer 2 from New England Biolabs (NEB), 200 μM ATP (NEB), and 658 U/mL T4 DNA Ligase (NEB). The tube was placed on a thermoshaker (21.5 °C, 30 min) then rinsed thrice in RB. The substrate was then added to the labeling tube, containing 1.8 μg/mL SAPE (Life Technologies) in RB, and placed on a thermoshaker (21.5 °C, 1500 rpm, 45 min) then rinsed thrice.

Fluorescence Imaging. For characterization and optimization, substrates were imaged on a Zeiss Axio Observer A1 inverted microscope. For fluorescence images, a broad-spectrum LED (X-CITE LED120, Excelitas Technologies) was used as a light source with a fluorescent filter, an Andor Clara CCD camera, and Andor SOLIS software used for image acquisition. Color bright-field images were acquired using a Nikon D7000 camera and Nikon Camera Control Pro 2 software. For miRNA studies, substrates were imaged on a GenePix 4400A Slide Scanner (molecular devices, 532 nm laser, full power, gain of 500, focal height of 150 μm, pixel resolution of 5 μm, and an Alexa568 filter).

Total RNA from Human Biological Samples. Total RNA from the breast tumor and NAT (500 ng) was purchased from BioChain. The patient was a 53 year-old female with moderately differentiated invasive lobular carcinoma. The human serum was purchased from BioIVT (Table S6) and clarified by centrifugation (3000g, 15 min, 15 °C), then aliquoted at 200 μL and stored at −20 °C until use. Total RNA was purified from the serum using the QIAGEN miRNeasy Serum/Plasma Advanced Kit (catalogue no. 217204) following the manufacturer's instructions, with minor modifications as outlined herein. After adding buffer RPL to the serum, 1000 amol of positive spike-in cel-miR-54 was added. Also, a double elution was performed to efficiently elute the total RNA: 20 μL of 1× TE for the first elution and 17 μL for the second. Two microliter were used for RNA yield quantification and quality control using a NanoDrop Spectrophotometer, and 32.5 μL were used in the miRNA assays. Total RNA was stored at −20 °C until use.

Statistical Data Analysis. Unpaired two-tailed t-tests were performed to determine the statistical significance between the means of all pairs of populations, as shown in Figure 5. The threshold significance level (α) was set to 0.05. Each data set (i.e., miRNA type) was analyzed individually, without assuming a consistent SD.

ASSOCIATED CONTENT

Ⓢ Supporting Information

The Supporting Information is available free of charge at https://pubs.acs.org/doi/10.1021/acssensors.0c02121.

Characterization and optimization studies, human donor information, and sequences for all nucleic acids used herein (PDF)

AUTHOR INFORMATION

Corresponding Author

Patrick S. Doyle − Department of Chemical Engineering, Massachusetts Institute of Technology, Cambridge, Massachusetts 02139, United States; Ⓞ orcid.org/0000-0003-2147-9172; Email: pdoyle@mit.edu

Authors

Dana Al Sulaiman − Department of Chemical Engineering, Massachusetts Institute of Technology, Cambridge,

Massachusetts 02139, United States; Ⓞ orcid.org/0000-0002-3185-6288

Sarah J. Shapiro − Department of Chemical Engineering, Massachusetts Institute of Technology, Cambridge, Massachusetts 02139, United States; Ⓞ orcid.org/0000-0003-2399-4928

Jose Gomez-Marquez − Little Devices Lab, Massachusetts Institute of Technology, Cambridge, Massachusetts 02139, United States

Complete contact information is available at:
https://pubs.acs.org/10.1021/acssensors.0c02121

Author Contributions

[#]D.A.S. and S.J.S. contributed equally. The manuscript was written through contributions of all the authors. All the authors have given approval to the final version of the manuscript.

Notes

The authors declare no competing financial interest.

REFERENCES

(1) Le Goff, G. C.; Srinivas, R. L.; Hill, W. A.; Doyle, P. S. Hydrogel Microparticles for Biosensing. *Eur. Polym. J.* **2015**, *72*, 386−412.

(2) Lee, H.; Srinivas, R. L.; Gupta, A.; Doyle, P. S. Sensitive and Multiplexed On-Chip MicroRNA Profiling in Oil-Isolated Hydrogel Chambers. *Angew. Chem., Int. Ed.* **2015**, *127*, 2507−2511.

(3) Nagarajan, M. B.; Tentori, A. M.; Zhang, W. C.; Slack, F. J.; Doyle, P. S. Nonfouling, Encoded Hydrogel Microparticles for Multiplex MicroRNA Profiling Directly from Formalin-Fixed, Paraffin-Embedded Tissue. *Anal. Chem.* **2018**, *90*, 10279−10285.

(4) Tentori, A. M.; Nagarajan, M. B.; Kim, J. J.; Zhang, W. C.; Slack, F. J.; Doyle, P. S. Quantitative and Multiplex MicroRNA Assays from Unprocessed Cells in Isolated Nanoliter Well Arrays. *Lab Chip* **2018**, *18*, 2410−2424.

(5) Lee, H. J.; Roh, Y. H.; Kim, H. U.; Kim, S. M.; Bong, K. W. Multiplexed Immunoassay Using Post-Synthesis Functionalized Hydrogel Microparticles. *Lab Chip* **2018**, *19*, 111.

(6) Al Sulaiman, D.; Chang, J. Y. H.; Ladame, S. Subnanomolar Detection of Oligonucleotides through Templated Fluorogenic Reaction in Hydrogels: Controlling Diffusion to Improve Sensitivity. *Angew. Chem., Int. Ed.* **2017**, *56*, 5247−5251.

(7) Chapin, S. C.; Appleyard, D. C.; Pregibon, D. C.; Doyle, P. S. Rapid MicroRNA Profiling on Encoded Gel Microparticles. *Angew. Chem., Int. Ed.* **2011**, *50*, 2289−2293.

(8) Shapiro, S. J.; Dendukuri, D.; Doyle, P. S. Design of Hydrogel Particle Morphology for Rapid Bioassays. *Anal. Chem.* **2018**, *90*, 13572−13579.

(9) Srinivas, R. L.; Johnson, S. D.; Doyle, P. S. Oil-Isolated Hydrogel Microstructures for Sensitive Bioassays On-Chip. *Anal. Chem.* **2013**, *85*, 12099−12107.

(10) Nagarajan, M. B.; Tentori, A. M.; Zhang, W. C.; Slack, F. J.; Doyle, P. S. Spatially Resolved and Multiplexed MicroRNA Quantification from Tissue Using Nanoliter Well Arrays. *Microsyst. Nanoeng.* **2020**, *6*, 51.

(11) Martinez, A. W.; Phillips, S. T.; Butte, M. J.; Whitesides, G. M. Patterned Paper as a Platform for Inexpensive, Low-Volume, Portable Bioassays. *Angew. Chem., Int. Ed.* **2007**, *46*, 1318−1320.

(12) Bhandari, P.; Narahari, T.; Dendukuri, D. Fab-Chips: A Versatile, Fabric-Based Platform for Low-Cost, Rapid and Multiplexed Diagnostics. *Lab Chip* **2011**, *11*, 2493−2499.

(13) Fang, X.; Wei, S.; Kong, J. Paper-Based Microfluidics with High Resolution, Cut on a Glass Fiber Membrane for Bioassays. *Lab Chip* **2014**, *14*, 911−915.

(14) Phillips, E. A.; Young, A. K.; Albarran, N.; Butler, J.; Lujan, K.; Hamad-Schifferli, K.; Gomez-Marquez, J. Ampli: A Construction Set for Paperfluidic Systems. *Adv. Healthcare Mater.* **2018**, *7*, 1800104.

(15) Yetisen, A. K.; Akram, M. S.; Lowe, C. R. Paper-Based Microfluidic Point-of-Care Diagnostic Devices. *Lab Chip* **2013**, *13*, 2210−2251.

(16) Martinez, A. W.; Phillips, S. T.; Nie, Z.; Cheng, C.-M.; Carrilho, E.; Wiley, B. J.; Whitesides, G. M. Programmable Diagnostic Devices Made from Paper and Tape. *Lab Chip* **2010**, *10*, 2499−2504.

(17) Martinez, A. W.; Phillips, S. T.; Butte, M. J.; Whitesides, G. M. Patterned Paper as a Platform for Inexpensive, Low-Volume, Portable Bioassays. *Angew. Chem., Int. Ed.* **2007**, *46*, 1318−1320.

(18) Reches, M.; Mirica, K. A.; Dasgupta, R.; Dickey, M. D.; Butte, M. J.; Whitesides, G. M. Thread as a Matrix for Biomedical Assays. *ACS Appl. Mater. Interfaces* **2010**, *2*, 1722−1728.

(19) Ali, M. M.; Aguirre, S. D.; Xu, Y.; Filipe, C. D. M.; Pelton, R.; Li, Y. Detection of DNA Using Bioactive Paper Strips. *Chem. Commun.* **2009**, *0*, 6640−6642.

(20) Hossain, S. M. Z.; Luckham, R. E.; McFadden, M. J.; Brennan, J. D. Reagentless Bidirectional Lateral Flow Bioactive Paper Sensors for Detection of Pesticides in Beverage and Food Samples. *Anal. Chem.* **2009**, *81*, 9055−9064.

(21) Hossain, S. M. Z.; Luckham, R. E.; Smith, A. M.; Lebert, J. M.; Davies, L. M.; Pelton, R. H.; Filipe, C. D. M.; Brennan, J. D. Development of a Bioactive Paper Sensor for Detection of Neurotoxins Using Piezoelectric Inkjet Printing of Sol-Gel-Derived Bioinks. *Anal. Chem.* **2009**, *81*, 5474−5483.

(22) Mateen, R.; Ali, M. M.; Hoare, T. A Printable Hydrogel Microarray for Drug Screening Avoids False Positives Associated with Promiscuous Aggregating Inhibitors. *Nat. Commun.* **2018**, *9*, 602.

(23) Owczarczak, A. B.; Shuford, S. O.; Wood, S. T.; Deitch, S.; Dean, D. Creating Transient Cell Membrane Pores Using a Standard Inkjet Printer. *J. Visualized Exp.* **2012**, *61*, No. e3681.

(24) Pepper, M. E.; Parzel, C. A.; Burg, T.; Boland, T.; Burg, K. J.; Groff, R. E. Design and Implementation of a Two-Dimensional Inkjet Bioprinter. In *2009 Annual International Conference of the IEEE Engineering in Medicine and Biology Society*; 2009; pp 6001−6005.

(25) Love, J. C.; Wolfe, D. B.; Jacobs, H. O.; Whitesides, G. M. Microscope Projection Photolithography for Rapid Prototyping of Masters with Micron-Scale Features for Use in Soft Lithography. *Langmuir* **2001**, *17*, 6005−6012.

(26) Ambros, V. The Functions of Animal MicroRNAs. *Nature* **2004**, *431*, 350−355.

(27) Bartel, D. P. MicroRNAs. *Cell* **2004**, *116*, 281−297.

(28) Swarup, V.; Rajeswari, M. R. Circulating (Cell-Free) Nucleic Acids − A Promising, Non-Invasive Tool for Early Detection of Several Human Diseases. *FEBS Lett.* **2007**, *581*, 795−799.

(29) Bye, A.; Røsjø, H.; Nauman, J.; Silva, G. J. J.; Follestad, T.; Omland, T.; Wisløff, U. Circulating MicroRNAs Predict Future Fatal Myocardial Infarction in Healthy Individuals - The HUNT Study. *J. Mol. Cell. Cardiol.* **2016**, *97*, 162−168.

(30) Halvorsen, A. R.; Helland, Å.; Gromov, P.; Wielenga, V. T.; Talman, M.-L. M.; Brunner, N.; Sandhu, V.; Børresen-Dale, A.-L.; Gromova, I.; Haakensen, V. D. Profiling of MicroRNAs in Tumor Interstitial Fluid of Breast Tumors − A Novel Resource to Identify Biomarkers for Prognostic Classification and Detection of Cancer. *Mol. Oncol.* **2017**, *11*, 220−234.

(31) Volinia, S.; Galasso, M.; Elena, M.; Wise, T. F.; Palatini, J.; Huebner, K. Breast Cancer Signatures for Invasiveness and Prognosis de Fi Ned by Deep Sequencing of MicroRNA. *Proc. Natl. Acad. Sci. U.S.A.* **2012**, *109*, 3024.

(32) Pritchard, C. C.; Cheng, H. H.; Tewari, M. MicroRNA Profiling: Approaches and Considerations. *Nat. Rev. Genet.* **2012**, *13*, 358−369.

(33) Sita-Lumsden, A.; Dart, D. A.; Waxman, J.; Bevan, C. L. Circulating MicroRNAs as Potential New Biomarkers for Prostate Cancer. *Br. J. Cancer* **2013**, *108*, 1925−1930.

(34) Ulivi, P.; Zoli, W. MiRNAs as Non-Invasive Biomarkers for Lung Cancer Diagnosis. *Molecules* **2014**, *19*, 8220.

(35) Mall, C.; Rocke, D. M.; Durbin-Johnson, B.; Weiss, R. H. Stability of MiRNA in Human Urine Supports Its Biomarker Potential. *Biomarkers Med.* **2013**, *7*, 623−631.

(36) Glinge, C.; Clauss, S.; Boddum, K.; Jabbari, R.; Jabbari, J.; Risgaard, B.; Tomsits, P.; Hildebrand, B.; Kääb, S.; Wakili, R.; Jespersen, T.; Tfelt-Hansen, J. Stability of Circulating Blood-Based MicroRNAs - Pre-Analytic Methodological Considerations. *PLoS One* **2017**, *12*, No. e0167969.

(37) de Puig, H.; Bosch, I.; Gehrke, L.; Hamad-Schifferli, K. Challenges of the Nano-Bio Interface in Lateral Flow and Dipstick Immunoassays. *Trends Biotechnol.* **2017**, *35*, 1169−1180.

(38) Fang, X.; Wei, S.; Kong, J. Paper-Based Microfluidics with High Resolution, Cut on a Glass Fiber Membrane for Bioassays. *Lab Chip* **2014**, *14*, 911−915.

(39) Konwarh, R.; Gupta, P.; Mandal, B. B. Silk-Microfluidics for Advanced Biotechnological Applications: A Progressive Review. *Biotechnol. Adv.* **2016**, *34*, 845−858.

(40) Mellors, J. S.; Gorbounov, V.; Ramsey, R. S.; Ramsey, J. M. Fully Integrated Glass Microfluidic Device for Performing High-Efficiency Capillary Electrophoresis and Electrospray Ionization Mass Spectrometry. *Anal. Chem.* **2008**, *80*, 6881−6887.

(41) Le Goff, G. C.; Lee, J.; Gupta, A.; Hill, W. A.; Doyle, P. S. High-Throughput Contact Flow Lithography. *Adv. Sci.* **2015**, *2*, 1500149.

(42) Palanichamy, J. K.; Rao, D. S. MiRNA Dysregulation in Cancer: Towards a Mechanistic Understanding. *Front. Genet.* **2014**, *5*, 54.

(43) Lugli, G.; Cohen, A. M.; Bennett, D. A.; Shah, R. C.; Fields, C. J.; Hernandez, A. G.; Smalheiser, N. R. Plasma Exosomal MiRNAs in Persons with and without Alzheimer Disease: Altered Expression and Prospects for Biomarkers. *PLoS One* **2015**, *10*, No. e0139233.

(44) Pandey, A. K.; Agarwal, P.; Kaur, K.; Datta, M. MicroRNAs in Diabetes: Tiny Players in Big Disease. *Cell. Physiol. Biochem.* **2009**, *23*, 221−232.

(45) Cheng, G. Circulating MiRNAs: Roles in Cancer Diagnosis, Prognosis and Therapy. *Adv. Drug Deliv. Rev.* **2015**, *81*, 75−93.

(46) Esquela-Kerscher, A.; Slack, F. J. Oncomirs - MicroRNAs with a Role in Cancer. *Nat. Rev. Cancer* **2006**, *6*, 259−269.

(47) Iorio, M. V.; Ferracin, M.; Liu, C.-G.; Veronese, A.; Spizzo, R.; Sabbioni, S.; Magri, E.; Pedriali, M.; Fabbri, M.; Campiglio, M.; Ménard, S.; Palazzo, J. P.; Rosenberg, A.; Musiani, P.; Volinia, S.; Nenci, I.; Calin, G. A.; Querzoli, P.; Negrini, M.; Croce, C. M. MicroRNA Gene Expression Deregulation in Human Breast Cancer. *Cancer Res.* **2005**, *65*, 7065−7070.

(48) Yan, L.-X.; Huang, X.-F.; Shao, Q.; Huang, M.-Y.; Deng, L.; Wu, Q.-L.; Zeng, Y.-X.; Shao, J.-Y. MicroRNA MiR-21 Overexpression in Human Breast Cancer Is Associated with Advanced Clinical Stage, Lymph Node Metastasis and Patient Poor Prognosis. *RNA* **2008**, *14*, 2348−2360.

(49) Qian, B.; Katsaros, D.; Lu, L.; Preti, M.; Durando, A.; Arisio, R.; Mu, L.; Yu, H. High MiR-21 Expression in Breast Cancer Associated with Poor Disease-Free Survival in Early Stage Disease and High TGF-B1. *Breast Cancer Res. Treat.* **2009**, *117*, 131−140.

(50) Asaga, S.; Kuo, C.; Nguyen, T.; Terpenning, M.; Giuliano, A. E.; Hoon, D. S. Direct Serum Assay for MicroRNA-21 Concentrations in Early and Advanced Breast Cancer. *Clin. Chem.* **2011**, *57*, 84−91.

(51) Usmani, A.; Shoro, A. A.; Shirazi, B.; Memon, Z.; Hussain, M. Mir-16: A Novel Hereditary Marker in Breast Cancer and Their Offspring. *J. Pak. Med. Assoc.* **2017**, *67*, 446−450.

(52) Xiang, M.; Zeng, Y.; Yang, R.; Xu, H.; Chen, Z.; Zhong, J.; Xie, H.; Xu, Y.; Zeng, X. U6 Is Not a Suitable Endogenous Control for the Quantification of Circulating MicroRNAs. *Biochem. Biophys. Res. Commun.* **2014**, *454*, 210−214.

(53) Wong, T.-S.; Liu, X.-B.; Wong, B. Y.-H.; Ng, R. W.-M.; Yuen, A. P.-W.; Wei, W. I. Mature MiR-184 as Potential Oncogenic MicroRNA of Squamous Cell Carcinoma of Tongue. *Clin. Cancer Res.* **2008**, *14*, 2588−2592.

(54) McDermott, A. M.; Kerin, M. J.; Miller, N. Identification and Validation of MiRNAs as Endogenous Controls for RQ-PCR in Blood Specimens for Breast Cancer Studies. *PLoS One* **2013**, *8*, No. e83718.

(55) Lange, T.; Stracke, S.; Rettig, R.; Lendeckel, U.; Kuhn, J.; Schlüter, R.; Rippe, V.; Endlich, K.; Endlich, N. Identification of MiR-16 as an Endogenous Reference Gene for the Normalization of Urinary Exosomal MiRNA Expression Data from CKD Patients. *PLoS One* **2017**, *12*, No. e0183435.

(56) Zhu, W.; Qin, W.; Atasoy, U.; Sauter, E. R. Circulating MicroRNAs in Breast Cancer and Healthy Subjects. *BMC Res. Notes* **2009**, *2*, 89.

(57) Bär, C.; Thum, T.; Gonzalo-Calvo, D. d. Circulating MiRNAs as Mediators in Cell-to-Cell Communication. *Epigenomics* **2019**, *11*, 111−113.

(58) Poel, D.; Buffart, T. E.; Oosterling-Jansen, J.; Verheul, H. M.; Voortman, J. Evaluation of Several Methodological Challenges in Circulating MiRNA QPCR Studies in Patients with Head and Neck Cancer. *Exp. Mol. Med.* **2018**, *50*, No. e454.

(59) Williams, Z.; Ben-Dov, I. Z.; Elias, R.; Mihailovic, A.; Brown, M.; Rosenwaks, Z.; Tuschl, T. Comprehensive Profiling of Circulating MicroRNA via Small RNA Sequencing of CDNA Libraries Reveals Biomarker Potential and Limitations. *Proc. Natl. Acad. Sci. U. S. A.* **2013**, *110*, 4255−4260.

(60) Helgeson, M. E.; Chapin, S. C.; Doyle, P. S. Hydrogel Microparticles from Lithographic Processes: Novel Materials for Fundamental and Applied Colloid Science. *Curr. Opin. Colloid Interface Sci.* **2011**, *16*, 106−117.

(61) De Jager, W.; Prakken, B. J.; Bijlsma, J. W. J.; Kuis, W.; Rijkers, G. T. Improved Multiplex Immunoassay Performance in Human Plasma and Synovial Fluid Following Removal of Interfering Heterophilic Antibodies. *J. Immunol. Methods* **2005**, *300*, 124−135.

(62) Tentori, A. M.; Nagarajan, M. B.; Kim, J. J.; Zhang, W. C.; Slack, F. J.; Doyle, P. S. Quantitative and Multiplex MicroRNA Assays from Unprocessed Cells in Isolated Nanoliter Well Arrays. *Lab Chip* **2018**, *18*, 2410−2424.

(63) Chen, C.; Ridzon, D. A.; Broomer, A. J.; Zhou, Z.; Lee, D. H.; Nguyen, J. T.; Barbisin, M.; Xu, N. L.; Mahuvakar, V. R.; Andersen, M. R.; Lao, K. Q.; Livak, K. J.; Guegler, K. J. Real-Time Quantification of MicroRNAs by Stem-Loop RT-PCR. *Nucleic Acids Res.* **2005**, *33*, No. e179.

(64) Ouyang, T.; Liu, Z.; Han, Z.; Ge, Q. MicroRNA Detection Specificity: Recent Advances and Future Perspective. *Anal. Chem.* **2019**, *91*, 3179−3186.

(65) Liang, R.-Q.; Li, W.; Li, Y.; Tan, C. Y.; Li, J. X.; Jin, Y. X.; Ruan, K. C. An Oligonucleotide Microarray for MicroRNA Expression Analysis Based on Labeling RNA with Quantum Dot and Nanogold Probe. *Nucleic Acids Res.* **2005**, *33*, No. e17.

(66) Zheng, W.; Yao, L.; Teng, J.; Yan, C.; Qin, P.; Liu, G.; Chen, W. Lateral Flow Test for Visual Detection of Multiple MicroRNAs. *Sens. Actuators, B* **2018**, *264*, 320−326.

(67) Gao, X.; Xu, H.; Baloda, M.; Gurung, A. S.; Xu, L.-P.; Wang, T.; Zhang, X.; Liu, G. Visual Detection of MicroRNA with Lateral Flow Nucleic Acid Biosensor. *Biosens. Bioelectron.* **2014**, *54*, 578−584.

(68) Šípová, H.; Zhang, S.; Dudley, A. M.; Galas, D.; Wang, K.; Homola, J. Surface Plasmon Resonance Biosensor for Rapid Label-Free Detection of Microribonucleic Acid at Subfemtomole Level. *Anal. Chem.* **2010**, *82*, 10110−10115.

(69) Degliangeli, F.; Kshirsagar, P.; Brunetti, V.; Pompa, P. P.; Fiammengo, R. Absolute and Direct MicroRNA Quantification Using DNA-Gold Nanoparticle Probes. *J. Am. Chem. Soc.* **2014**, *136*, 2264−2267.

(70) Su, S.; Fan, J.; Xue, B.; Yuwen, L.; Liu, X.; Pan, D.; Fan, C.; Wang, L. DNA-Conjugated Quantum Dot Nanoprobe for High-Sensitivity Fluorescent Detection of DNA and Micro-RNA. *ACS Appl. Mater. Interfaces* **2014**, *6*, 1152−1157.

(71) Zhu, D.; Zhang, L.; Ma, W.; Lu, S.; Xing, X. Detection of MicroRNA in Clinical Tumor Samples by Isothermal Enzyme-Free Amplification and Label-Free Graphene Oxide-Based SYBR Green I Fluorescence Platform. *Biosens. Bioelectron.* **2015**, *65*, 152−158.

(72) Qavi, A. J.; Kindt, J. T.; Gleeson, M. A.; Bailey, R. C. Anti-DNA:RNA Antibodies and Silicon Photonic Microring Resonator Arrays Enable the Ultrasensitive, Multiplexed Detection of Micro-RNAs. *Anal. Chem.* **2011**, *83*, 5949−5956.

(73) Cacheux, J.; Bancaud, A.; Leichlé, T.; Cordelier, P. Technological Challenges and Future Issues for the Detection of Circulating MicroRNAs in Patients With Cancer. *Front. Chem.* **2019**, *7*, 815.

(74) Lee, H.; Shapiro, S. J.; Chapin, S. C.; Doyle, P. S. Encoded Hydrogel Microparticles for Sensitive and Multiplex MicroRNA Detection Directly from Raw Cell Lysates. *Anal. Chem.* **2016**, *88*, 3075−3081.

(75) Ng, E. K. O.; Li, R.; Shin, V. Y.; Jin, H. C.; Leung, C. P. H.; Ma, E. S. K.; Pang, R.; Chua, D.; Chu, K.-M.; Law, W. L.; Law, S. Y. K.; Poon, R. T. P.; Kwong, A. Circulating MicroRNAs as Specific Biomarkers for Breast Cancer Detection. *PLoS One* **2013**, *8*, No. e53141.

(76) Sempere, L. F.; Christensen, M.; Silahtaroglu, A.; Bak, M.; Heath, C. V.; Schwartz, G.; Wells, W.; Kauppinen, S.; Cole, C. N. Altered MicroRNA Expression Confined to Specific Epithelial Cell Subpopulations in Breast Cancer. *Cancer Res.* **2007**, *67*, 11612−11620.

(77) Khalighfard, S.; Alizadeh, A. M.; Irani, S.; Omranipour, R. Plasma MiR-21, MiR-155, MiR-10b, and Let-7a as the Potential Biomarkers for the Monitoring of Breast Cancer Patients. *Sci. Rep.* **2018**, *8*, 17981.

(78) Zheng, M.; Sun, X.; Li, Y.; Zuo, W. MicroRNA-145 Inhibits Growth and Migration of Breast Cancer Cells through Targeting Oncoprotein ROCK1. *Tumor Biol.* **2016**, *37*, 8189−8196.

(79) Chapin, S. C.; Doyle, P. S. Ultrasensitive Multiplexed MicroRNA Quantification on Encoded Gel Microparticles Using Rolling Circle Amplification. *Anal. Chem.* **2011**, *83*, 7179−7185.